Title	Characterization and reactivity of charcoal from high temperature pyrolysis (800–1600°C)
Author(s)	Surup, Gerrit Ralf; Nielsen, Henrik K.; Heidelmann, Markus; Trubetskaya, Anna
Publication Date	2018-09-22
Publication Information	Surup, Gerrit Ralf, Nielsen, Henrik Kofoed, Heidelmann, Markus, & Anna, Trubetskaya. (2019). Characterization and reactivity of charcoal from high temperature pyrolysis (800–1600°C). Fuel, 235, 1544-1554. doi: https://doi.org/10.1016/j.fuel.2018.08.092
Publisher	Elsevier
Link to publisher's version	https://doi.org/10.1016/j.fuel.2018.08.092
Item record	http://hdl.handle.net/10379/14568
DOI	http://dx.doi.org/10.1016/j.fuel.2018.08.092

Characterization and reactivity of charcoal from high temperature pyrolysis (800-1600°C)

Gerrit Ralf Surup[a], Henrik Kofoed Nielsen[a], Markus Heidelmann[b], Anna Trubetskaya[c,*]

[a]*Department of Engineering Sciences, University of Agder, 4879 Grimstad, Norway*
[b]*Interdisciplinary Center for Analytics on the Nanoscale, University of Duisburg-Essen, 47057 Duisburg, Germany*
[c]*Mechanical Engineering Department, National University of Ireland Galway, Galway, Ireland*

Abstract

This study presents the effect of wood origin and heat treatment temperature on the CO_2 reactivity, nanostructure and carbon chemistry of chars prepared at 800, 1200, and 1600°C in slow pyrolysis reactors. The structure of charcoal was characterized by transmission electron microscopy, Raman spectroscopy, mercury intrusion porosimetry and N_2 adsorption. The CO_2 reactivity of char was investigated by thermogravimetric analysis. Results showed that spruce and oak chars have similar reactivity at all heat treatment temperatures. The oak char prepared at 1600°C contained long and flat graphene layers and interplanar distance that is similar to graphite and thus, was more ordered than the spruce char. The TEM analysis showed that charcoal had structural characteristics of non-graphitizing carbon. Thus, increasing heat treatment temperature increases the graphitization of char structure, leading to the reactivity that is nearly similar to that of low reactive metallurgical coke.

*Corresponding author. anna.trubetskaya@nuigalway.ie

The wood origin, heat treatment temperature, nanostructure, differences in porosity and pore size of char influenced the CO_2 reactivity less than the differences in CO_2 concentrations.
Keywords: charcoal, high-temperature pyrolysis, CO_2 reactivity, non-graphitizing carbon, low heating rate

---

Nomenclature

A	Relative area	X	Conversion
A_i	Pre-exponential factor (s^{-1})	m	Mass (kg)
C	Constant	p	pressure (Pa)
C_{fix}	Fixed carbon yield (wt.% on dry basis)	SSA	Specific surface area (m^2 g^{-1})
		Greek symbols	
D	Diameter (m)	γ	surface tension (N $m^{-}1$)
E_a	Activation Energy (kJ mol^{-1})	κ	Heating rate (K s^{-1})
L_a	Mean cristal size in a-direction (Å)	λ	Wavenumber (cm^{-1})
		ρ	Density (kg m^{-3})
R	Gas constant (J mol^{-1} K^{-1})	Θ	angle of contact (°)
T	Temperature (K)	**Subscripts**	
V	Pore volume (mm^3)	a	average
V	Volume (m^3)	cum	cumulative

md	median	s	solid phase
p	pore		

1. Introduction

Ferroalloy production is energy-intensive, consuming large amounts of both electricity and coke. Coke is used in ferroalloy production to reduce metal oxides to the base metal. Development of cost-effective, renewable reductants is environmentally desirable because global ferroalloy production releases about 55 Mt of CO_2 emissions annually [1]. Using carbon sources from renewable, plant-based materials has potential to replace fossil-based reducing agents and effectively reduce CO_2 emissions. In recent years, much progress has been made on conversion of plant-based materials to carbonaceous char materials; some of these materials may have potential as reductants. However, metallurgical production continues to rely on fossil-based reductants due to limited knowledge of char properties and conditions required to produce chars with acceptable reactivity, and high costs.

Transportation of carbon reductants from Asia and South America creates additional economic and environmental challenges and thus, alternative options in Norway can be resorted [2]. In Norway, vast forest resources covering 12.8 million hectares with significant volumes of wood in the order of 6-8 million m^3 is harvested annually while wood growth increase by 25 million m^3 annually. This suggests that biomass can be an abundant source of carbon reductants in ferroalloy production [3, 4]. Norway spruce, Scots pine and birch form 45 %, 30 % and 16 % of forestry in Norway respectively [5]. There are different types of wood that can be converted into charcoal, of

which wood residuals, consisting of limbs, tops, and stems are especially promising candidates for the use as carbonaceous reductants in ferroalloy industries because of low cost and high abundance [6]. The most important properties of the carbonaceous reductant are high reactivity, high conversion and low levels of impurities (such as sulphur and phosphorus) [7]. Low ash content is important, as each additional percent of ash in carbonaceous reductant increases slag volume by about 10-15 kg t^{-1} of ferroalloy, thereby increasing the electric power required for smelting [8]. Different types of wood contain various amounts of mineral compounds depending on the growth conditions. In general, hardwood ash contains a greater amount of K and P and less Ca and Si than softwood ash [9]. There are notable differences in the same genus of softwood, but less variation among hardwood species [10, 11]. The distribution of lignocellulosic compounds shows significant variations between wood fractions (e.g. root, stem, and branch) [12]. The amount of extractives is greater in bark than in stemwood, whereas needles are rich in lipophilic extractives, especially in waxes [13–15]. Wood branches and roots contain a greater amount of galactan, xylan and lignin compared to glucomannan rich stemwood [16]. The high reactivity of biocarbon-based reductant may be advantageous in some cases within the ferroalloy industries, however, the use of a reductant more reactive than metallurgical coke may increase maintenance costs due to the decreased electrical conductivity [17, 18]. Therefore, reductant reactivity becomes a key variable that must be understood in potential replacements for metallurgical coke. Likewise, the effect of porosity and nanostructure in biocarbon-based reductants must also be considered. The increase in porosity of carbonaceous reductants increases

the reactivity and thus the porous plant-based materials are advantageous in ferroalloy industries [19, 20]. Charcoal porosity and pore size vary from 40 to 50 % and from 20 to 30 μm [21]. In particular, charcoal from hardwood species is less porous than charcoal from softwood leading to the lower reactivity at high temperature pyrolysis [22]. Low interplanar distances (close to that of graphite) and high periodicity lead to lower oxidation of carbon materials, while the more bent graphene layers might enhance the reactivity [23, 24]. The graphitizing carbons are non-porous with relatively high densities, whereas non-graphitizing carbonaceous materials have low density due to the high microporosity [25]. The non-graphitizability of charcoal is related to its porous structure [26, 27]. The nanostructure of charcoal from pyrolysis at temperatures > 2500°C is observed to be similar to natural graphite, whereas charcoal prepared at lower temperatures exhibits a structure resembling glassy carbon [28, 29]. Treatment at temperatures greater than 1250°C will be required to produce non-graphitizing carbons suitable as metallurgical coke. Despite the arguments in favor of high temperature charcoal, the majority of previous investigations have studied charcoals produced at temperatures < 1000°C [30–33].

In summary, biocarbon-based materials have potential as environmentally benign replacements to fossil-based reductants, but knowledge of relationship between wood type, temperature and charcoal properties is limited. Therefore, in this study, the impacts of heat treatment temperature (800-1600°C), wood origin, porosity and nanostructure on the CO_2 reactivity were investigated in the slow pyrolysis reactor to simulate the conditions in industrial-scale coke production. The specific objectives of this study were

to: (1) develop structure-property relationships governing the CO_2 reactivity of charcoal, and (2) determine the treatment conditions and wood composition which decrease char reactivity to levels that are suitable for application in ferroalloy industries.

2. Materials and methods

Norway spruce and oak were chosen for the charcoal study. Fuel selection was based on the differences in ash composition and plant cell compounds (cellulose, hemicellulose, lignin, extractives). Norway spruce is low in ash and with lower potassium and calcium contents than oak, whereas oak is low in lignin content. Char samples were generated in the slow pyrolysis reactor at 800 and 1200°C. The char sample generated at 1200°C was further heated to 1600°C in the high-temperature furnace. The charcoal samples were crushed to a fine powder in a mortar with a ceramic pestle. The char samples were investigated under CO_2 gasification condition in a thermogravimetric analyzer. Reactivities of activated charcoal, metallurgical coke, and spruce and oak char samples were compared using reaction rates calculated from the derived kinetic parameters. Mercury intrusion porosimetry, N_2 adsorption, transmission electron microscopy (TEM) analysis and Raman spectroscopy were performed to characterize the effect of temperature and feedstock on the char carbon structure, surface properties and nanostructure.

2.1. Carbon material characterization

Norway spruce (*Picea abies*) and oak (*Quercus petraea*) from Dømmesmoen (Grimstad, Norway) were harvested in 2012 and 2016 respectively. The age

of the Norway spruce was ≈ 39 years, whereas the oak was ≈ 46 years. Both the Norway spruce and oak trees were chipped by a disc chipper to 5-20 mm and dried at 60°C. Metallurgical coke and activated charcoal were provided by Norsk Koksverk A/S (Mo i Rana, Norway). Prior to characterization, biomass samples were divided into six equal fractions using a riffler. The biomass samples were comminuted to < 0.8 mm in a laboratory-scale mill POLYMIX PX-MFC 90 D (KINEMATICA, Switzerland).

2.2. Slow pyrolysis reactor

The charcoal samples were generated in the slow pyrolysis reactor, as shown in Figure 1. The reactor can be operated at temperatures up to 1350°C and heating rates up to 20°C min^{-1}. The pyrolysis setup encloses a two-stage cooling system with a condensation collector and a pyrolysis gas sampling unit. The pyrolysis retort (inner diameter: 75 mm, height: 150 mm, wall thickness: 2 mm) is made of SiC material. The sample temperature was monitored by a thermocouple type S (max. 1600°C). The connection pipes (inner diameter: 10 mm) between the retort and the condensation unit were made of quartz glass. The connection pipes were heated up to 350 °C by a heating tape HBQ (Hillesheim, Germany) and a temperature regulator MC1 (HORST GmbH, Germany) to minimize the condensation and thermal decomposition of tars. The volume flow of the N_2 gas was measured by the flowmeter HFC-202 (Teledyne, USA). The reactor was continuously purged by nitrogen at a constant flow rate of 100 ml min^{-1}. The temperature control system was based on the LabView software (Version 8.6). The sample mass of 60 g for each experiment was selected. The wood sample was distributed homogeneously in the reactor's retort, pre-heated in nitrogen at 10°C min^{-1}

up to 160°C and kept at that temperature for 30 min.

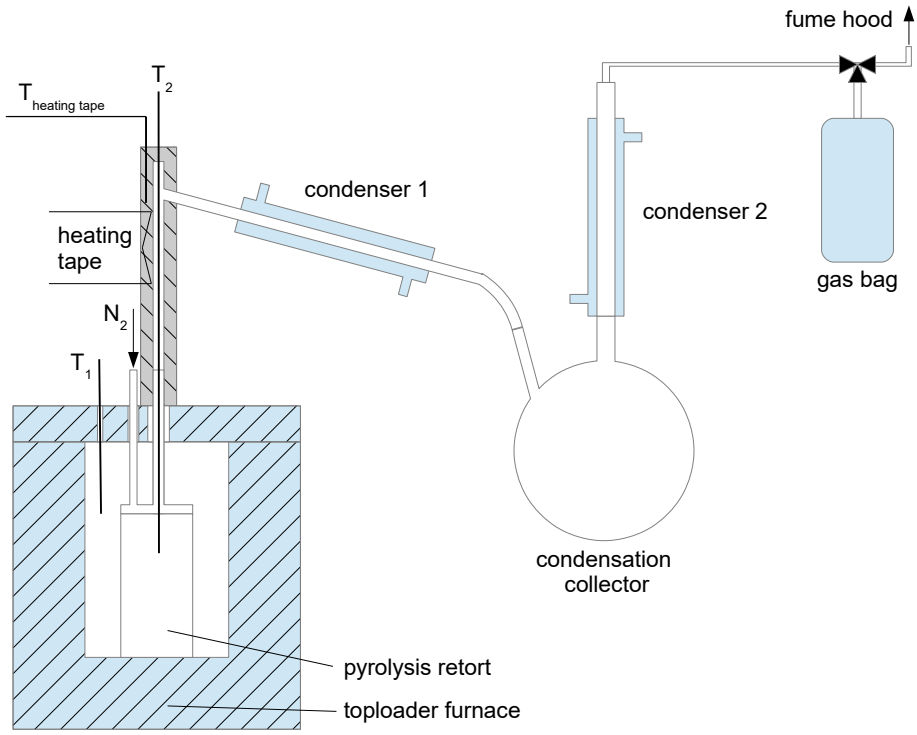

Figure 1: Slow pyrolysis reactor at University of Agder.

The dried wood was further heated at 10°C min^{-1} up to 800 or 1200°C and kept at the final temperature for about 1 h to ensure the complete conversion. After the heating program was finished, the furnace was turned off and the charcoal sample was cooled overnight in N_2 (0.3 l min^{-1}). Samples were stored in sealed plastic containers.

2.3. High-temperature furnace

The charcoal samples were further treated in the high-temperature furnace LHTG 200-300/20-1G (Carbolite Gero, Germany). The furnace can

be operated at temperatures up to 1800°C and at heating rates up to 20°C min^{-1}. Prior to each experiment, 5 g of the char sample was loaded into the A_2O_3 crucible (Almath Crucibles Ltd, UK) placed in the graphite retort middle. Prior to pyrolysis, the furnace was repeatedly evacuated and purged by argon. The char sample was heated at 10°C min^{-1} up to 1600°C and kept at that temperature for 2 h. The sample was cooled to room temperature at a heating rate of 20°C min^{-1} and stored in sealed plastic containers.

2.4. Char analysis

Elemental analysis. The elemental analysis was performed on Analyser Series II (Perkin Elmer, USA). Acetanilide was used as a reference standard. The ash content was determined using a standard ash test at 550°C, according to the procedure described in DIN EN 14775.

Thermogravimetric analysis. The thermal decomposition of char samples was determined using an atmospheric thermogravimetric instrument STARe System (Mettler Toledo, USA). The reactivity of char in 20 % or 100 % volume fraction CO_2 (20 cm^3 min^{-1} of CO_2 and 80 cm^3 min^{-1} of N_2 or 100 cm^3 min^{-1} of CO_2 measured at 20°C and 101.3 kPa) was determined by loading 5 mg of sample in Al_2O_3 crucible. The char samples were firstly heated up to 110°C and kept for 30 min isothermally for drying. The dried samples were subsequently heated to 1100°C at a constant heating rate of 10 °C min^{-1}. The kinetic parameters of char samples were derived by the integral method presented by Coats and Redfern [34]. Through integral transformation and mathematical approximation, the linear equation was expressed in the form:

$$ln\left(-\frac{ln(1-X)}{T^2}\right) = ln\left(\frac{A_i \cdot R}{\kappa \cdot E_a}\right) - \frac{E_a}{R \cdot T} \quad (1)$$

In equation 1, κ is the heating rate and R is the gas constant. A plot of ln(-ln(1-X) T^{-2}) versus T^{-1} gives a straight line whose slope and intercept determine the values of the activation energy (E_a) and pre-exponential factor (A_i). The reactivities of char samples were compared using reaction rates calculated from the derived kinetic parameters (A_i and E_a) at a fixed gasification temperature of 1000°C.

Raman spectroscopy. Raman spectroscopy was performed using an inVia Raman microscope (Renishaw, UK) operating with a 514 nm laser line at a power of 30 mW. The measurements were performed in static mode with a center at 1600 cm^{-1}, resulting in a 960-2200 cm^{-1} spectral region. The laser power was set to 100 % in the software and roughly 30 % in the hardware by using a filter. 1 s exposure time was used in normal confocality mode. A 20x lens and 8-15 μm step size (X and Y directions) was used for mapping, to generate 100-200 spectra/image for each char sample. Cosmic rays were removed and the data was subjected to multivariate noise filtering using the WiRE chemometrics package version 3.0 (Renishaw, UK). Spectra were saved as text files and processed via the free, open-source MatLab script provided by the Vibrational Spectroscopy Core Facility at Umeå University (www.kbc.umu.se/english/visp/download-visp/). The following parameters were used for spectra pre-processing: asymmetrical least squares baseline correction with lambda = 20000000 and p = 0.001 [35]; Savitzky-Golay smoothing with the first polynomial order and frame rate of 3 [36]. Spectra were total area normalized in the entire spectral range. The corrected spectra from each mapping were then averaged to create a final composite curve for the peak deconvolution. No spectral scaling was performed. Deconvolution

of the Raman spectra was conducted using the peak fit pro tool in the OriginPro software (OriginLab, USA) by combination of nine Gaussian-shaped bands (S_L, S, D_S, D, A_1, A_2, G_G, G_L, and D') following Smith et al. [37]. The mean crystal size in the *a*-direction (L_a) with the fitting constants C_0 = -12.6 nm and C_1 = 0.033, which are valid for the laser wavelength from 400 to 700 nm, is given by [38]:

$$L_a = \frac{C_0 + C_1 \lambda_L}{A_D / A_{G_L}} \tag{2}$$

N_2 adsorption analysis. The specific surface area (SSA) of biomass chars was determined based on N_2 adsorption at the boiling point (77 K). To prevent gas adsorption, the char samples were degassed under vacuum at 350°C. The multipoint Brunauer-Emmett-Teller (BET) theory with seven points in the range of p/p_0 from 0.06 to 0.3 was applied on the NOVA 2000e instrument (Quantachrome, Germany). BET equation was used to determine the specific surface area [39].

Transmission electron microscopy. Prior to microscopy, char samples were kept at 350°C for 6 h in a thermogravimetric instrument to reduce the amount of volatiles. Samples were ground in a mortar to ensure a homogeneous particle distribution, sonified in deionized water for 30 min, wet dispersed on a lacey carbon copper grid and dried at room temperature for 20 min. Char nanostructure was studied using a Jeol 2200fs operated at 200 keV, equipped with an Oxford Instruments X-Max SDD EDS detector. The curvature of a single graphene sheet is defined in equation 3:

$$Curvature = \frac{Length}{Fiber\ \ length} \tag{3}$$

The length is a straight line that connects both ends of a graphene sheet. The fiber length is the contour or arc length, as shown in the supplemental material (Figure S-1). Both length and fiber length were estimated by Gatan Digital Micrograph software according to the method of Müller et al. [40]. Portions of the image with visible graphene layers were magnified to a size of 10 nm x 10 nm, and both length and fiber length were manually determined by the software ruler which draws a straight or contour line to connect both ends of a graphene sheet.

Mercury intrusion porosimetry. The pore size distribution and porosity of char samples were determined by a Pascal mercury intrusion porosimeter system equipped with two instruments. Porosity in the ultramacro- and macropore regions was measured by Pascal 140 porosimeter (Micromeritics, Germany) at the low pressures (up to 400 kPa). The Pascal 440 porosimeter equipped with a dilatometer (Micromeritics, Germany) was used to determine the pore size from 1.8 to 7500 nm at high pressures up to 400 MPa. To access the pores and voids within biomass particles, the samples were degassed at room temperature prior to the measurement. Prior to the porosity analysis, wood fractions were dried at 50°C in an oven desiccator for 48 h.

Pore volume and size. The pore sizes in the char were distinguished into three categories: micropores (1.8-80 nm), mesopores (80-500 nm) and macropores (0.5-58 μm) [41, 42]. The pore volume can be derived from the quantity of intruded mercury. The pore size distribution is determined according to the Washburn equation [43]:

$$D_p = -\frac{4\gamma cos\Theta}{p} \tag{4}$$

In equation 4, Θ is assumed to be equal to 141° [44] and γ is equal to 0.48 N m^{-1} [41]. The median pore diameter (D_{md}) is defined as the pore diameter at which 50 % of total intrusion was reached. The average pore diameter (D_{pa}) is calculated, assuming that all pores are cylindrical, in equation 5:

$$D_{pa} = -\frac{4V_{cum}}{SSA} \tag{5}$$

The cumulative pore volume distribution is calculated in equation 6:

$$V_{cum}(D) = \frac{-dV_p}{dlogD_p} \tag{6}$$

Helium pycnometry. The skeletal density is defined in accordance with DIN 66137 (Part 2) standard by equation 7:

$$\rho_s = \frac{m_s}{V_s} \tag{7}$$

The calculation of skeletal density excludes the porosity within the particles and the interparticle voids. The skeletal density was determined using a helium pycnometer (POTOTEC GmbH, Germany) at room temperature.

3. Results

3.1. Biomass characterization

The ultimate and proximate analysis of metallurgical coke, activated charcoal, and wood was carried out at Eurofins Lidköping and shown in Table 1.

Table 1: Proximate, ultimate and ash analyses of feedstocks.

Fuel	Norway spruce	Oak	Activated charcoal	Metallurgical coke
Proximate and ultimate analysis, (wt.% on dry basis)				
Moisture[a]	8.6	7.6	3.8	0.6
Ash (550 °C)	0.8	1.6	8.6	11.8
Volatiles	80.6	82.6	10.3	3
C_{fix}	18.6	15.8	81.1	85.2
HHV[b]	20.3	19.3	30.5	27.9
LHV[b]	18.5	17.5	30.2	27.8
C	53.2	50.6	82.6	85.6
H	6.1	6.1	1.5	0.3
N	0.1	0.2	0.8	1.8
S	0.06	0.02	0.9	0.6
Cl	0.04	0.02	0.02	0.03
Ash compositional analysis, (mg kg^{-1} on dry basis)				
Al	40	20	4500	12000
Ca	2300	3600	4900	6400
Fe	200	50	3700	6300
K	800	1500	1900	1700
Mg	250	300	850	1300
Na	<50	<50	1100	1100
P	200	250	400	400
Si	550	550	31000	27000
Ti	50	50	200	550

[a] wt. % (as received)

[b] in MJ kg^{-1}

The compositional analysis of biomass (cellulose, hemicellulose, acid-soluble lignin, acid-insoluble lignin, and extractives) was conducted according to NREL technical reports [45–47] and Thammasouk et al. [48], and shown in Table 2.

Table 2: Composition of Norway spruce and oak, calculated in percentage based on dry basis (wt. %).

Biomass	**Cellulose**	**Hemicellulose**	**Lignin**		**Extractives**
			acid insoluble	**acid soluble**	
Norway spruce	37.8	25	27.9	0.7	7.8
Oak	36.7	18.7	19.4	2.5	11

3.2. Char reactivity

Figure 2 shows differential weight loss curves (DTG) for the 20 % and 100 % volume fraction CO_2 gasification of char samples, metallurgical coke and activated charcoal. The relative importance of external diffusion on the overall char gasification in the TG experiments was evaluated by comparison of the observed maximal reaction rate (r_{max}, % min^{-1}) with the calculated diffusion rate (r_{diff}, % min^{-1}) of CO_2 in the supplemental material (equation 1). The calculated r_{max}/r_{diff} ratio showed that the gasification reaction in the TG analysis was influenced only by chemical kinetic limitations, as shown in the supplemental material (Table S-3). The DTG curves show both a single broad peak and a double peak in CO_2 gasification, indicating a heterogeneous char mixture with respect to the composition. A double DTG peak indicates a combination of two constituents with different reactivity [49, 50]. The minor shoulder DTG peak at nearly the same temperature range from 810 to 825°C was related to the reactivity of heavy hydrocarbon compounds [51]. The CO_2 gasification of most char samples and activated charcoal took place at nearly the same temperature range from 700 to 1200°C, whereas metallurgical coke reacted at higher temperatures. The reactivities of char from spruce and oak

were nearly identical, confirming previous results of Trubetskaya [29].

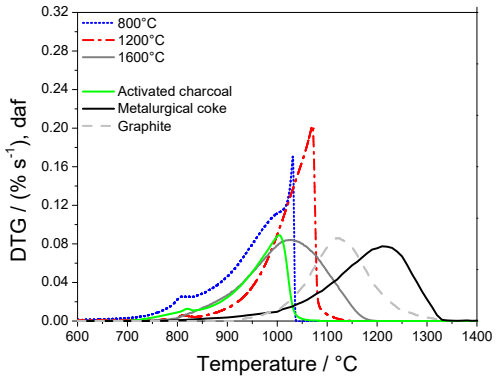

2(a): Spruce char (20 % CO_2 + 80 % N_2)

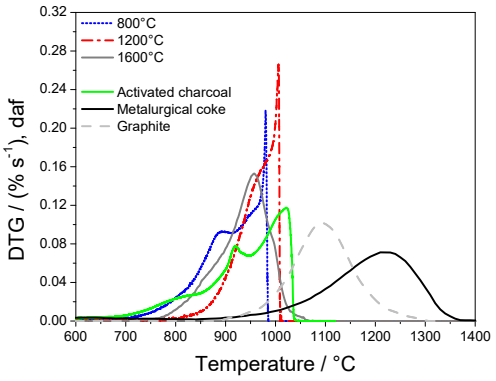

2(b): Spruce char (100 % CO_2)

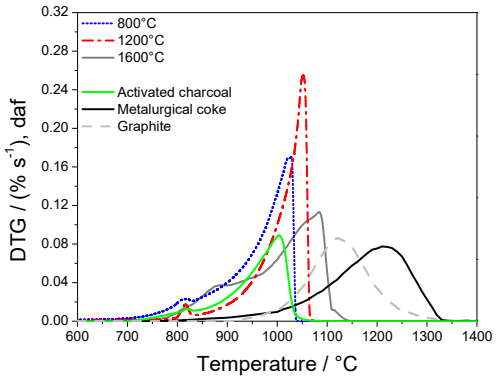

2(c): Oak char (20 % CO_2 + 80 % N_2)

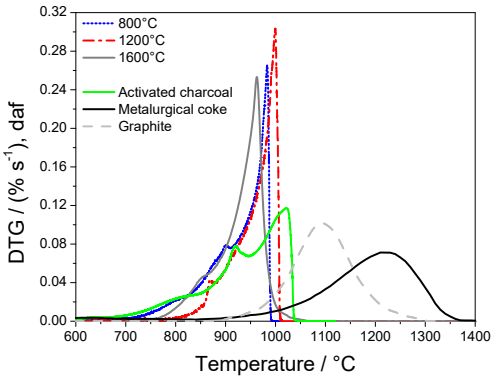

2(d): Oak char (100 % CO_2)

Figure 2: (a)-(d) DTG curves of metallurgical coke, activated charcoal, spruce and oak chars prepared at 800, 1200, and 1600°C and reacted in 20 % volume fraction CO_2 + 80 % volume fraction N_2 and 100 % CO_2.

The maximum reaction rate of oak char from pyrolysis at 1600°C in 20 % CO_2 gasification was about 100°C greater than char produced at 800°C. The maximum reaction rate of oak char at 1600°C in 100 % CO_2 gasification was about 20°C lower than that of oak char produced at 800°C. The maximal

reaction rate of char samples reacted in 20 % or 100 % CO_2 changed significantly, based on the kinetic parameters in the supplemental material (Tables S-1 and S-2). The increasing CO_2 concentration led to the greater reactivity of both spruce and oak chars, confirming previous results of Cetin et al. [52]. Increasing heat treatment temperature resulted in a greater shift of maximum reaction rate from 50 °C at 800 °C to 70 °C at 1200 and 1600 °C. Interestingly, the reactivity of metallurgical coke in 20 % and 100 % CO_2 remained only slightly changed. The results show that differences in heat treatment temperature and feedstock origin have less influence on char reactivity than the CO_2 concentration, and will be discussed below.

3.3. Elemental analysis

Figure 3 shows a Van Krevelen plot of original Norway spruce and oak and their chars, activated charcoal, and metallurgical coke. The results in Figure 3 indicate that spruce char obtained from pyrolysis at 800 and 1200°C contained more oxygen than oak char. The increased heat treatment temperature from 1200 to 1600°C led to an increase in carbon content of both chars and thus the elemental composition of char samples was comparable to the composition of metallurgical coke. The activated charcoal contained more oxygen and hydrogen than chars obtained from pyrolysis at 1200°C.

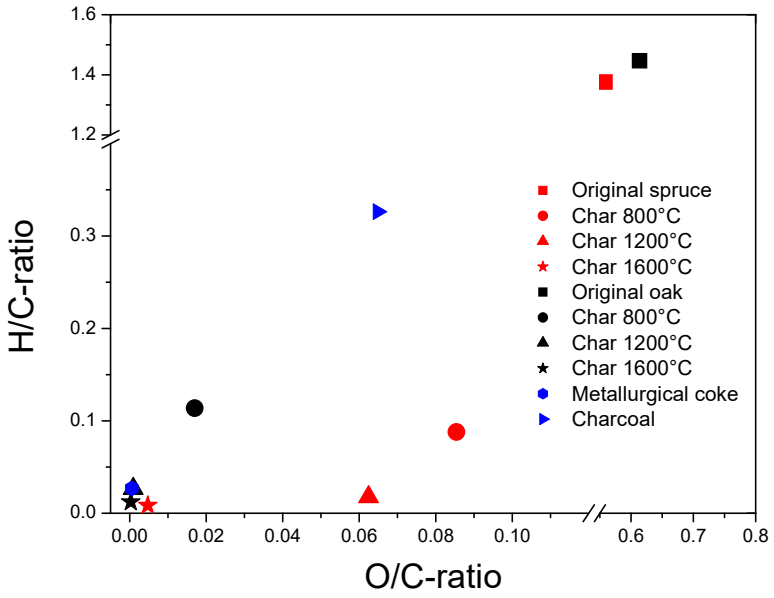

Figure 3: Van Krevelen plot of metallurgical coke, activated charcoal, Norway spruce and oak chars prepared at 800, 1200, and 1600°C.

3.4. Nanostructure

The nanostructure of the spruce and oak chars generated at 800, 1200, and 1600°C was studied by TEM, as shown in Figure 4. Both charcoal samples exhibited a common structure of amorphous carbon at 800 and 1200°C, whereas a mixture of amorphous carbon and nano-crystalline graphite was observed at 1600°C. In addition, spruce char showed two types of amorphous carbon structure at 1600°C. The short graphene sheets of the spruce char merged, forming a continuous surface with a large number of crystallites, similar to the pyrolytic glassy carbon and lignin char, as shown in Figure 4(e) [53, 54].

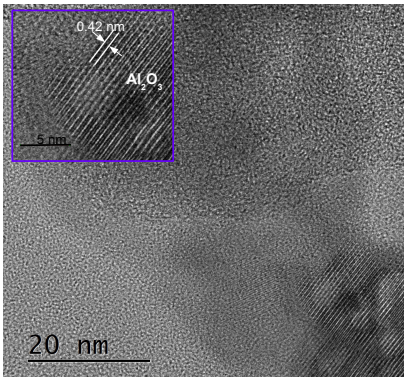

4(a): Spruce char (800°C)

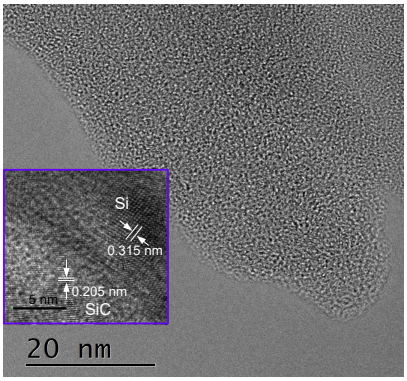

4(b): Oak char (800°C)

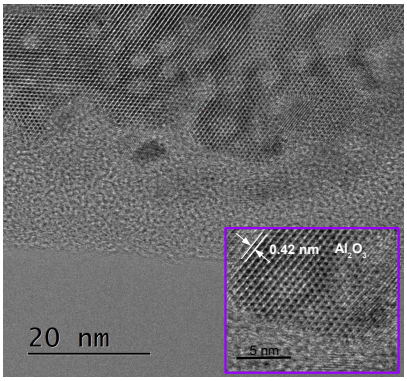

4(c): Spruce char (1200°C)

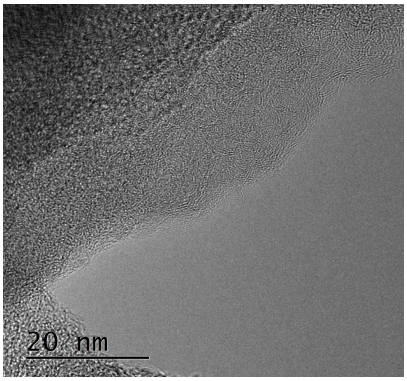

4(d): Oak char (1200°C)

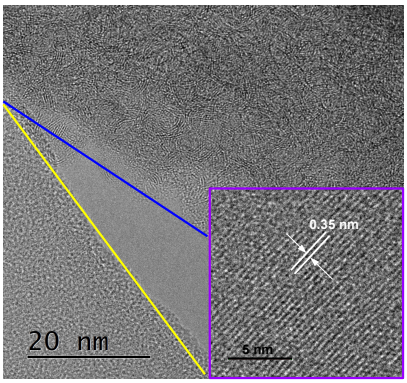

4(e): Spruce char (1600°C)

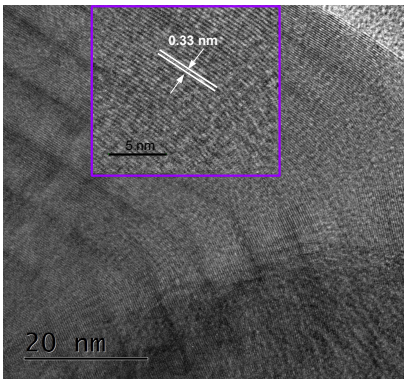

4(f): Oak char (1600°C)

Figure 4: TEM images of char generated from spruce and oak. In Figures (a)-(c), (e) and (f) the distance between graphene layers, Al_2O_3, SiC and Si was measured in the enlarged image (purple rectangle). In Figure (e) the areas of different carbon types are marked with blue and yellow lines.

Another type of amorphous carbon structure with more curved graphene layers was indicated on the spruce char surface and mixed with the nano-crystalline graphite. Figure 4(f) shows the nanostructure of oak char generated at 1600°C that mainly consists of nano-crystalline graphite with 22-26 layers of straight graphene layers arranged in an interconnected ribbon-like geometry [55]. The oak char nanostructure was similar to that of the crystalline carbon membrane [56]. The bent graphene layers of graphitized char contain carbon with hexagonal graphene layers [57] and a mean interplanar distance of 0.33 nm that indicates the highest degree of graphitization (graphite $\approx$ 0.335 nm) [58]. The spruce char generated at 1600°C had a less ordered structure with the mean interplanar distance of 0.35 nm, as shown in Figure 4(e). The differences in the nanostructure of spruce and oak chars generated at 1600°C suggest that the feedstock composition has an influence on the char properties in high-temperature pyrolysis. The additional structures, detected by the TEM analysis of spruce and oak chars, were related to the presence of inorganic matter such as Al_2O_3 and Si [59, 60]. In addition, TEM analysis showed that all char samples contained a small amount of SiC particles from the reactor's retort which could form the sp^3 diamond-like carbon in high-temperature pyrolysis [61, 62].

3.5. Porosity and pore size

Table 3 summarizes the characteristics of spruce and oak chars generated at 800, 1200, and 1600°C with regards to porosity, pore size and specific surface area. The porosity by skeleton density of spruce and oak chars measured by the mercury intrusion system was in the range from 70 to 78.8 % and from 61.5 to 47.2 %. Previous studies showed that the compositional

differences led to lower porosity and greater apparent density of Eucalyptus charcoal compared to Acacia charcoal [63]. In the present study, the increase in porosity of spruce char is caused by the progressive removal of volatiles from pores, and the physical and chemical condensation of the remaining skeletal char structure with increasing heat treatment temperature, confirming previous results of Brewer at al. [32]. In contrast, the porosity of oak char samples decreased, probably due to the high alkali metal content in oak chars. The residual alkali metals (K^+ and Ca^{2+}) in oak char samples decreased the porosity to such extent that the active surface area was also decreased with increasing heat treatment temperature [64]. The greater alkali metal content in oak chars could also lead to the formation of charcoal with the different pore size and shape than during pyrolysis of low ash-containing spruce.

Table 3 shows that both spruce and oak chars possessed a high ratio of macropores. The macroporosity of the oak char (93-95 %) was significantly greater than that of spruce char (57-60.3 %). The micro- and mesoporosity of the spruce char ranged from 4 to 6 %, whereas the oak char possessed greater proportion of micro- (23 %) and mesopores (16.7-20 %). The results also correspond to the greater total pore area of oak char samples (57.3-69.8 $m^2\ g^{-1}$) than that of the spruce char (10.7-11.8 $m^2\ g^{-1}$). In the present study, the formation of all pores in charcoal was a function of feedstock origin and less dependent on the heat treatment temperature respectively. The total pore area determined by mercury intrusion porosimetry was lower than that determined by N_2 adsorption because mercury porosimetry primarily determined macropores, whereas N_2 adsorption measured micro- and mesopores [65, 66]. The results showed that the SSA of spruce and oak char samples determined

by N_2 adsorption decreased significantly from 196 and 495 $m^2\ g^{-1}$ to 3 and 11 $m^2\ g^{-1}$ with the increased heat treatment temperature, as reported by Hussein et al. [67].

Table 3: Porosity and pore size of spruce and oak char, characterized by mercury intrusion porosimeter and BET surface area (SSA) and pore size (DFT method) of chars, determined by N_2 adsorption $m^2\ g^{-1}$.

Parameter	**Spruce**			**Oak**			**Metallurgical**	**Activated**
	800°C	**1200°C**	**1600°C**	**800°C**	**1200°C**	**1600°C**	**coke**	**charcoal**
Mercury intrusion porosimetry								
Porosity by Hg intrusion, %	70	74.5	78.8	61.5	58.2	47.2	39.7	14
Porosity by skeleton density, %	78.5	81.4	79.5	68.5	60.5	65.5	47.8	33
Inaccessible porosity, %	8.8	7	0.6	7.1	2.2	18.2	8.1	20
Macropores, %	93	95	93	60.3	57	57	87	97
Mesopores, %	6	4	6	16.7	20	20	10	3
Micropores, %	1	1	1	23	23	23	3	
V_{cum}, $mm^3\ g^{-1}$	1917	2636.8	2788.5	1163	1065	1232	403	146
Total pore surface area, $m^2\ g^{-1}$	11.4	11.8	10.7	57.3	69.8	65.3	5.9	0.2
Average pore diameter, μm	0.7	0.9	1	0.1	0.1	0.1	0.3	2.3
Median pore diameter, μm	6.9	7.7	6.9	1.1	0.9	0.9	16.2	21.8
N_2 adsorption								
BET surface area (SSA), $m^2\ g^{-1}$	196	97.2	3	495	80	11	2.8	0.3
Pore size, nm	0.6	0.7	1.3	0.6	0.7	0.9	0.9	0.9

The reduction in the surface area was probably caused by the continuous growth of graphene sheets with the increasing heat treatment temperature, leading to the micropore coalescence [68]. The average pore size of the spruce and oak char samples varied from 0.7 to 2.3 nm using mercury intrusion porosimeter whereas the average pore size of both spruce and oak chars varied only slightly from 0.6 to 1.3 nm when N_2 adsorption was used. This indicated no significant changes in all pore sizes. In addition, the pore size

and specific surface area of oak char prepared at 1600°C were similar to the values reported for metallurgical coke ($2.8\,m^2\ g^{-1}$; 0.9 nm).

3.6. Raman spectroscopy

Raman spectroscopy was carried out to examine primary differences in the carbon structure of char samples. The calculated integrated peak area ratio (A_{S_L}/A_{G_L}) in Figure 5 and supplementary Table S-4 showed that the spruce char samples obtained a greater amount of carboxylates than the oak char, whereas the A_{S_L}/A_{G_L} ratio of oak char generated at 1600°C was the lowest (0.04) due to the low content of acetyl groups [69]. All char samples based on the A_D/A_{G_L} ratios exhibited a common structure of amorphous carbon and nano-crystalline graphite, as discussed by Ferrari and Robertson [70]. The pyrolysis at 800 and 1200°C formed a less graphitic charcoal structure (A_D/A_{G_L}: 2.3-2.5) than the pyrolysis at 1600°C (A_D/A_{G_L}: 1.7-1.9), corresponding to previous results of Trubetskaya et al. [22]. The average extensions of graphene stacks (L_a) from the Raman bands in spruce and oak chars generated at 800 and 1200°C (1.7-1.9 nm) were less than those in the charcoal from pyrolysis at 1600°C (2.3-2.6 nm). The size of one aromatic ring is 0.25 nm [71], and therefore, the size of PAHs in the char (800-1600°C) is equivalent to approximately 7-10 aromatic rings. Moreover, the average extension of graphene stacks (L_a) in all char samples was quantitatively similar to that of commercial carbon black (Printex XE2: 2.5 nm) and biomass soot (2.1-2.6 nm) and different from the graphite structure (5.6 nm) [72, 73].

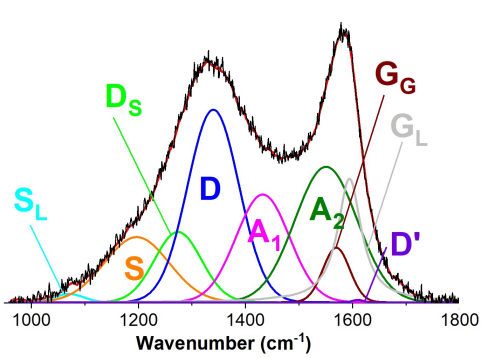

5(a): Spruce char (800°C)

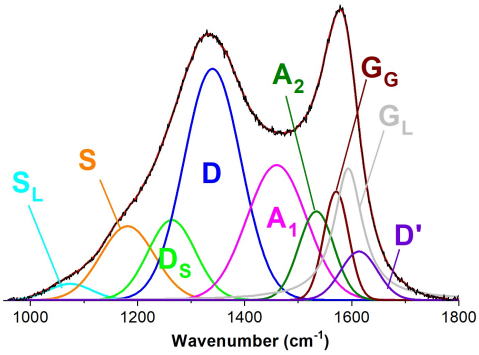

5(b): Oak char (800°C)

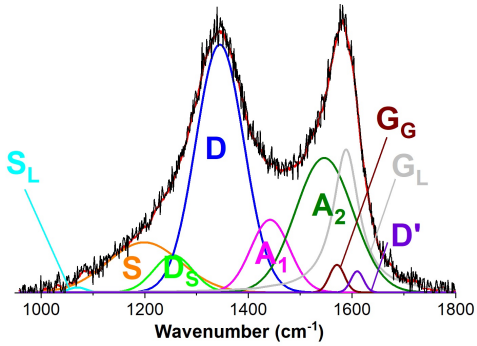

5(c): Spruce char (1200°C)

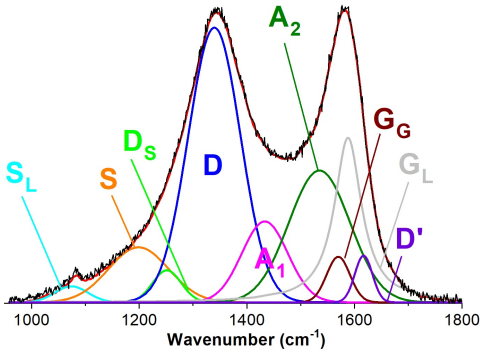

5(d): Oak char (1200°C)

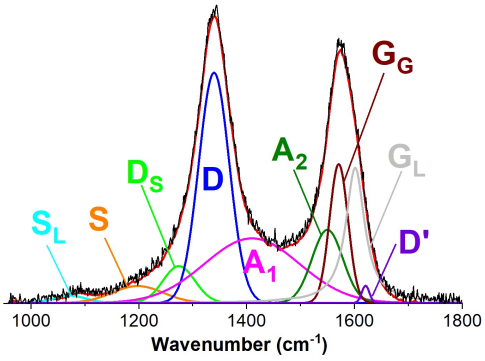

5(e): Spruce char (1600°C)

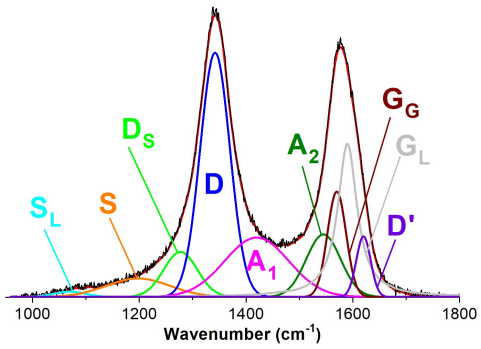

5(f): Oak char (1600°C)

Figure 5: (a)-(f) Deconvolution of Raman spectrum of Norway spruce and oak chars from pyrolysis at 800, 1200, and 1600°C.

4. Discussion

The thermogravimetric experiments demonstrated larger influence of CO_2 concentration on the intrinsic reactivity of char samples than the heat treatment temperature and feedstock origin. The reactivity of char can be affected by differences in carbon chemistry, ash composition, nanostructure, heat treatment temperature and surface area characteristics of char samples. Raman spectroscopy results showed that char samples from pyrolysis at 800, 1200, and 1600°C exhibited a structure resembling carbon black based on the A_D/A_{G_L} ratios (1.7-2.6). The ash content of original spruce (0.8 wt. %) was twice lower than in the original oak. Thus, based on ash content alone it might be expected that spruce char should be less reactive than the oak char. However, the inorganic matter of both spruce and oak chars remained small, as shown in the supplemental material (Figure S-23). Knudsen et al. [74] experimentally showed that at high temperatures, KCl sublimation and potassium silicates reactions are dominant during devolatilization, depending on the availability of Si, Cl, Ca and Mg in the original fuel. The lower Cl content in the wood might indicate that potassium was released in the form of KOH or to a minor extent in the form of KCl [75]. The reactivities of spruce and oak chars remained similar at 800 and 1200°C. This indicates that neither carbon structure nor ash composition had a strong influence on the observed differences in char reactivity.

Previous studies on charcoal from pyrolysis at temperatures < 1000°C showed that nanostructure and CO_2 reactivity are interrelated considerations. In the present study, all charcoal samples exhibited shorter and less curved graphene layers and less recognizable crystalline structure, indicat-

ing either greater porosity or larger fraction of amorphous carbon than in coal chars [76]. This indicates that biomass chars consist of non-graphitizing carbons [77–79]. The results showed that the differences in nanostructure of spruce and oak char samples from pyrolysis at 1600°C were large. The oak char nanostructure was similar to that of glassy carbon, as reported by Jenkins et al. [80]. The TEM analysis of oak char graphitic ribbons from pyrolysis at 1600°C showed that the mean interplanar distance of graphene layers (0.33 nm) was similar to graphite (0.335 nm). The spruce char samples exhibited heterogeneous structure of amorphous carbon and nano-crystalline graphite corresponding to the double DTG peak in Figure 2. A double DTG peak in spruce char samples indicated the presence of a carbon constituent with similar reactivity to graphite and a more reactive carbon structure with similar reactivity to biomass soot samples [73]. The lower oxygen content in wood than that in herbaceous biomass inhibited the cross-linking and repolymerization reactions and therefore enhanced the coalescence of crystallites, leading to the charcoal graphitization [81]. The oxygen-containing functional groups remaining in charcoal are located at the edges of aromatic layers which hinder the alignment of graphene layers during pyrolysis [79]. Thus, based on oxygen content alone it might be expected that charcoal from softwood pyrolysis is more graphitic than hardwood charcoal. However, the nanostructure of oak char from pyrolysis at 1600°C was more graphitic than that of spruce char. This is due to the catalytic effect of alkali on the oak charcoal graphitization that is especially pronounced at high temperatures (1000-1600°C) [82, 83]. Interestingly, the short graphene layers of spruce char could enhance the reactivity, whereas the straight and long graphene layers of

oak char are expected to decrease the char reactivity. However, the reactivity of spruce and oak chars were similar.

The increased heat treatment temperatures led to greater char porosity in pyrolysis at temperatures 300-700°C [32]. In the present study, the char porosity measured by mercury intrusion porosimetry varied among spruce and oak chars, but changed only slightly with the increased heat treatment temperature. Moreover, the spruce chars obtained less micro- and mesopores than the oak chars, indicating a strong influence of the feedstock origin on the char porosity. The specific surface area of spruce char prepared at 1600°C was 9 times smaller than that of char from pyrolysis at 800°C, whereas the spruce char prepared at 800°C was 4 times more reactive than char from pyrolysis at 1600°C in 20 % CO_2 gasification. The oak char generated at 800°C was twice more reactive than char from pyrolysis at 1600°C, whereas the specific surface area of char from 800°C pyrolysis was 8 times greater than the SSA of char prepared at 1600°C. This indicates that the heat treatment temperature has a small influence on the CO_2 reactivity of charcoal samples determined by N_2 adsorption.

The oak and spruce chars prepared at 800°C were 106 and 3 times more reactive respectively in 100 % CO_2 atmosphere than the chars in 20 % CO_2 gasification, indicating a major influence of CO_2 concentration on the char reactivity. The decrease in CO_2 concentration leads to the decrease in maximum reaction rate [84, 85]. In the present work, the linear correlation between reaction rate and partial pressure could not be established based on the experimental results (Table S-4) and calculations in the supplemental material (equation 3). Moreover, as it was mentioned above, the gasification

reaction in the TG analysis was influenced only by chemical kinetic limitations. Thus, the CO_2 concentration becomes the dominating factor governing gasification reactivity. The metallurgical coke in 20 % CO_2 gasification was 5 times less reactive than spruce and oak char samples from pyrolysis at 1600°C. The reactivity of metallurgical coke remained unchanged with increasing CO_2 concentration, whereas the reactivity of activated charcoal changed in a similar manner as the reactivity of spruce and oak chars from pyrolysis at 800°C. This shows that the further increase in heat treatment temperature could increase the char graphitization, leading to the development of a structure that is more similar to low reactive metallurgical coke.

5. Conclusion

The novelty of this work relies on the fact that char from wood consists mainly of non-graphitizing carbon. The results indicated that both char samples from spruce and oak contained mostly nano-crystalline graphite at 1600°C. However, the oak char was significantly more graphitic than the spruce char at 1600°C. At lower temperatures, both chars formed less ordered structure that is similar to amorphous carbon.

The major difference in the char morphology was related to the formation of a high ratio of micro- and mesopores in oak pyrolysis, whereas the spruce chars contained mainly macropores. The differences in micropore size of spruce and oak chars determined by N_2 adsorption were small. In contrast, the average pore size of oak char was 10 times smaller than that of spruce char using mercury intrusion porosity. The pore size analysis showed that the N_2 adsorption and mercury intrusion porosimetry methods are complemen-

tary for quantifying charcoal porosity characteristics at micro- to macropore scales.

The thermogravimetric analysis results showed that the char reactivity towards CO_2 depends mainly on the CO_2 concentration and less on the heat treatment temperature, ash composition and carbon structure. The more graphitic structure of oak char from pyrolysis at 1600°C with a smaller interplanar distance, long and flat graphene layers showed a similar reactivity to the less ordered oak char. Both char samples were significantly more reactive in a 100 % CO_2 atmosphere than in 20 % CO_2 gasification emphasizing the role of CO_2 concentration on the char reactivity. The charcoal from pyrolysis at 800°C showed a similar reactivity to the activated charcoal, whereas the charcoal prepared at 1600°C was more reactive than metallurgical coke. This work indicated that the increase in a heat treatment temperature will lead to the further deactivation of char with the structure that is similar to low reactive metallurgical coke.

Acknowledgements

The authors gratefully acknowledge financial support from Elkem AS, Saint Gobain Ceramic Materials AS, Eramet Norway AS, Kempe Foundation, Björn Wahlströms, and Jernkontoret Stiftelsen. The authors acknowledge the facilities and technical support of Dr. Andras Gorzsas at Umeå University. The German Federal Government, Federal State of Nordrhein-Westfalen, Deutsche Forschungsgemeinschaft (DFG) are acknowledged for their contribution toward the establishment of the Interdisciplinary Center for Analytics on the Nanoscale in the University of Duisburg-Essen. Gundula

Stein and Viktor Scherf from GNF Berlin-Adlershof e.V. are acknowledged for many discussions on N_2 adsorption analysis. We acknowledge Raymond Mclnerney from University of Limerick for the article proof-reading.

References

[1] Holappa L, Towards sustainability in ferroalloy production, J South African Inst Min Metal 110 (12) (2010) 1–8.

[2] Monsen B, Tangstad M, Midtgaard H, Use of charcoal in silicomanganese production, 10^{th} Int Ferroalloys Congress INFACON X. Transformation through Technology 68 (2004) 155–64.

[3] Borrelli P, Panagos P, Langhammer J, Apostol B, Schütt B, Assessment of the cover changes and the soil loss potential in European forestland: First approach to derive indicators to capture the ecological impacts on soil-related forest ecosystems, Ecol Indic 60 (2016) 1208–20.

[4] Sjølie HK, Latta GS, Adams DM, Solberg B, Impacts of agent information assumptions in forest sector modeling, J Forest Economics 17 (2011) 169–284.

[5] Wang L, Dibdiakova J, Gjolsjo S, Report on Solid Biofuels from Forest-Fuel Specification and Quality Assurance, Norwegian Forest and Landscape Institute 8 (2014) 1–45.

[6] Wesenbeeck SV, Wang L, Ronsse F, Prins W, Skreiberg Ø, Charcoal "Mines" in the Norwegian Woods, Fuel 30 (2016) 7959–70.

[7] Pistorius PC, Reductant selection in ferro-alloy production: The case for the importance of dissolution in the metal, J South African Inst Min Met 1 (2002) 33–6.

[8] Sahajwalla V, Dubikova M, Khanna R, Reductant characterisation and selection: implications for ferroalloys processing, 10^{th} Int Ferroalloys Congress INFACON X. Transformation through Technology 68 (2004) 351–62.

[9] Pitman RM, Wood ash use in forestry - a review of the environmental impacts, Forestry 79 (5) (2006) 563–88.

[10] Naylor L, Schmidt E, Agricultural use of wood ash as a fertiliser and limiting material, TAPPI J 69 (1986) 114–9.

[11] Naylor L, Schmidt E, Paper mill wood ash as a fertiliser and limiting material, TAPPI J 72 (1989) 199–206.

[12] Gustafsson G, Heartwood and lightwood formation in Scots pine - A physological approach. PhD thesis, Swedish University of Agricultural Sciences, 2001.

[13] Myeong S, Han SH, Shin SJ, Analysis of Chemical Compositions and Energy Contents of Different Parts of Yellow Poplar for Development of Bioenergy Technology, J Korean For Soc 99 (5) (2010) 706–10.

[14] Backlund I, Cost-effective Cultivation of Lodgepole Pine for Biorefinary Applications. PhD thesis, Swedish University of Agricultural Sciences, 2013.

[15] Koch P, Lodgepole pine in North America: Nonwood products characterization of tree parts, Forest Prod Soc, 1996.

[16] Hakkila P, Utilization of residual biomass, Springer, 1989.

[17] Yamagishi K, Endo K, Saga J, A comprehensive analysis of the furnace interior for high-carbon ferrochromium, 1^{th} Int Ferroalloys Congress INFACON 74. Transformation through Technology (1974) 143–7.

[18] De Waal A, Barker IJ, Rennie MS, Klopper J, Groeneveld BS, Electrical Factors Affecting the Economic Optimization of Submerged-arc Furnaces, 6^{th} Int Ferroalloys Congress INFACON 6. Transformation through Technology 1 (1974) 247–52.

[19] Pochart G, Joncourt L, Touchard N, Perdon C, Metallurgical benefit of reactive high grade ore in manganese alloys manufacturing, INFACON XI (2007) 217–29.

[20] Longbottom RJ, Monaghan BJ, Chowdhury AA, Reid MH, Zhang G, Mahoney MR and etc., Effect Mineral Matter on the Reactivity of Coke and its Replication in a Coke Analogue, ISIJ Int 56 (9) (2016) 1553–8.

[21] Standish N, Tanjung AFA, Gasification of single wood charcoal particles in CO_2, Fuel 67 (1988) 666–72.

[22] Trubetskaya A, Fast pyrolysis of biomass at high temperatures. PhD thesis, Technical University of Denmark, 2016.

[23] Hurt RH, Structure, properties, and reactivity of solid fuels, 27^{th} Symposium on Combust (1998) 2887–904.

[24] Liati A, Eggenschwiler PD, Schreiber D, Zelenay V, Ammann M, Variations in diesel soot reactivity along the exhaust after-treatment system, based on the morphology and nanostructure of primary soot particles, Combust Flame 160 (3) (2013) 671–81.

[25] Ion I, Kovalev Y, Banciu C, Pasuk I, Kuklin A, Structural studies of carbon materials by sans-technique, Rom J Phys 51 (7) (2006) 783–9.

[26] Ishimaru K, Vystavel T, Bronsveld P, Hata T, Imamura Y, Hosson JD, Diamond and pore structure observed in wood charcoal, J Wood Sci 47 (2001) 414–6.

[27] Hata T, Yamane T, Kobayashi E, Imamura Y, Ishihara S, Microstructural investigation of wood charcoal made by spark plasma sintering, J Wood Sci 44 (1998) 332–4.

[28] Harris PJF, New Perspectives on the Structure of Graphitic Carbons, Crit Rev Sold State Mat Sci 30 (2005) 235–53.

[29] Surup GR, Timko MT, Deike R, Schubert D, Foppe M, Trubetskaya A and etc., The effect of feedstock origin and temperature on the structure and reactivity of char from pyrolysis at 1300-2800°C, Fuel accepted.

[30] Antal MJ, Grønli M, The art, science, and technology of charcoal production, Ind Eng Chem Res 42 (2003) 1619–40.

[31] Bourke J, Manley-Harris M, Fushimi C, Dowaki K, Nunoura T, Antal MJ, Do All Charcoals Have the Same Chemical Structure? 2. A Model of the Chemical Structure of Carbonized Charcoal, Ind Eng Chem Res 46 (18) (2007) 5954–67.

[32] Brewer CE, Chuang VJ, Masiello CA, Gonnermann H, Gao X, Dugan B and etc., New approaches to measuring biochar density and porosity, Biomass Bioenergy 66 (2014) 176–85.

[33] Griessacher T, Antrekowitsch J, Steinlechner S, Charcoal from agricultural residues as alternative reducing agent in metal recycling, Biomass Bioenergy 39 (2012) 139–46.

[34] Coats AW, Redfern JP, Kinetic Parameters from Thermogravimetric Data, Nature 201 (1964) 68–9.

[35] Eilers PHC, Parametric time WarpIng, Analyt Chem 76 (2) (2004) 404–11.

[36] Savitzky A, Golay MJE, Smoothing and differentiation of data by simplified least squares procedures, Analyt Chem 36 (8) (1964) 1627–39.

[37] Smith MW, Dallmeyer I, Johnson TJ, Brauer CS, McEwen JS, Espinal JF, Garcia-Perez M, Structural analysis of char by Raman spectroscopy: Improving band assignments through computational calculations from first principles, Carbon 100 (2016) 678–92.

[38] Matthews MJ, Pimenta MA, Dresselhaus G, Origin of dispersive effects of the Raman D band in carbon materials, Phys Rev B 59 (10) (1999) R6585–88.

[39] Brunauer S, Emmett PH, Teller E, Adsorption of Gases in Multimolecular Layers, J Am Chem Soc 60 (2) (1938) 309–19.

[40] Müller JO, Su DS, Wild U, Schlögl R, Bulk and surface structural investigations of diesel engine soot and carbon black, Phys Chem Chem Phys 9 (2007) 4018–25.

[41] Plötze M, Niemz P, Porosity and pore size distribution of different wood types as determined by mercury intrusion porosimetry, Europ J Wood Wood Product 69 (4) (2011) 649–57.

[42] Yin J, Song K, Lu Y, Zhao G, Yin Y, Comparison of changes in micropores and mesopores in the wood cell walls of sapwood and heartwood, Wood Sci Technol 49 (2015) 987–1001.

[43] Washburn EW, Note on a method of determining the distribution of pore sizes in a porous material, Proc Natl Acad Sci 7 (1921) 115–6.

[44] Junghaus K, Niemz P, Bächle F, Untersuchungen zum Einfluss der thermischen Vergütung auf die Porosität von Fichtenholz, Holz Roh Werkst 63 (3) (2005) 243–4.

[45] Sluiter A, Hames B, Ruiz R, Scarlata C, Sluiter J, Templeton D et al., Determination of Structural Carbohydrates and Lignin in Biomass. Golden (CO): National Renewable Energy Laboratory; 2011 July Report No. NREL/TP-510-42618. Contract No.: DE-AC36-08-GO28308 .

[46] Willför S, Hemming J, Leppänen AS, Analysis of extractives in different pulps - Method development, evaluation, and recommendations. Finland: Åbo Akademi University, Laboratory of Wood and Paper Chemistry; 2004-2009 Report No. B1 of the EU COST E41 action "Analytical tools with applications for wood and pulping chemistry" .

[47] Hames B, Ruiz R, Scarlata C, Sluiter J, Sluiter A, Preparation of Samples for Compositional Analysis. Golden (CO): National Renewable Energy Laboratory; 2011 June Report No. NREL/TP-510-42620. Contract No.: DE-AC36-99-GO10337 .

[48] Thammasouk K, Tandjo D, Penner MH, Influence of Extractives on the Analysis of Herbaceous Biomass, J Agric Food Chem 45 (1997) 437–43.

[49] Abian M, Jensen AD, Glarborg P, Alzueta MU, Soot Reactivity in Conventional Combustion and Oxy-fuel Combustion Environments, Energy Fuels 26 (8) (2012) 5337–44.

[50] Russell NV, Beeley TJ, Man CK, Gibbins JR, Williamson J, Development of TG measurements of intrinsic char combustion reactivity for industrial and research purposes, Fuel Process Tech 57 (2) (1998) 113–30.

[51] Zhang D, Ma Y, Zhu M, Nanostructure and oxidative properties of soot from a compression ignition engine: The effect of a homogeneous combustion catalyst, Proc Combust Inst 34 (2013) 1869–76.

[52] Cetin E, Moghtaderi B, Gupta R, Wall TF, Biomass Gasification Kinetics: Influences of Pressure and Char Structure, Comb Sci Tech 177 (4) (2005) 765–91.

[53] Jurkiewicz K, Pawlyta M, Zygadlo D, Chrobak D, Duber S, Wrzalik R and etc., Evolution of glassy carbon under heat treatment: correlation structure-mechanical properties, J Mater Sci 53 (2018) 3509–23.

[54] Li Y, Hu YS, Chen L, Li H, Huang X, A superior low-cost amorphous carbon anode made from pitch and lignin for sodium-ion batteries, J Mat Chem A 4 (2016) 96–104.

[55] Jenkins GM, Kawamura K, Polymeric Carbons - Carbon Fibre, Glass and Char, Cambridge University Press, 1976.

[56] Wollbrink A, Volgmann K, Koch J, Kanthasamy K, Tegenkamp C, Li Y and etc., Amorphous, turbostratic and crystalline carbon membranes with hydrogen selectivity, Carbon 106 (2016) 93–105.

[57] Welz S, McNallan MJ, Gogotsi Y, Carbon structures in silicon carbide derived carbon, J Mat Proc Tech 179 (2006) 11–22.

[58] Zhang ZL, Brydson R, Aslam Z, Reddy S, Brown A, Westwood A and etc., Investigating the structure of non-graphitising carbons using electron energy loss spectroscopy in the transmission electron microscope, Carbon 49 (2011) 5049–63.

[59] Gogotsi Y, Welz S, Ersoy DA, McNallan MJ, Conversion of silicon carbide to crystalline diamond-structured carbon at ambient pressure, Nature 411 (2000) 283–7.

[60] Aramesh M, Tran PA, Ostrikov K, Prawer S, Conformal nanocarbon coating of alumina nanocrystals for biosensing and bioimaging, Carbon 122 (2017) 422–7.

[61] Kiselev NA, Hutchison JL, Roddatis VV, Stepanova AN, Aksenova LL, Rakova EV and etc., TEM and HREM of diamond crystals grown on

Si tips: structure and results of ion-beam-treatment, Micron 36 (2000) 81–8.

[62] Ischenko V, Jang YS, Kormann M, Greil P, Popovska N, Zollfrank C and etc., The effect of SiC substrate microstructure and impurities on the phase formation in carbide-derived carbon, Carbon 49 (2011) 1189–98.

[63] Kumar M, Gupta RC, Influence of carbonization conditions on physical properties of Acacia and Eucalyptus wood chars, Trans Ind Inst Met 46 (6) (1993) 345–52.

[64] Branca C, Iannace A, Di Blasi C, Devolatilization and combustion kientics of Quercus Cerris, Energy Fuels 21 (2007) 1078–1084.

[65] Illingworth J, Williams PT, Rand B, Characterisation of biochar porosity from pyrolysis of biomass flax fibre, J Energy Inst 86 (2) (2013) 63–70.

[66] Giesche H, Mercury porosimetry: a general (practical) overview, Part part Syst Charact 23 (1) (2006) 9–19.

[67] Hussein A, Larachi F, Ziegler D, Alamdari H, Effects of heat treatment and acid washing on properties and reactivity of charcoal, Biomass Bioenergy 90 (2016) 101–13.

[68] Kercher AK, Nagle DC, Microstructural evolution during charcoal carbonization by X-ray diffraction analysis, Carbon 41 (2003) 15–27.

[69] Sun Y, Cheng J, Hydrolysis of lignocellulosic materials for ethanol production: a review, Biores Tech 83 (2002) 1–11.

[70] Ferrari AC, Robertson J, Raman spectroscopy of amorphous, nanostructured, diamond-like carbon, and nanodiamond, Phil Trans R Soc Lond 362 (2004) 2477–512.

[71] Hayashida K, Nagaoka S, Ishitani H, Growth and oxidation of graphitic crystallites in soot particles within a laminar diffusion flame, Fuel 128 (2014) 148–54.

[72] Jawhari T, Roid A, Casado J, Raman spectroscopic characterization of some commercially available carbon black materials, Carbon 33 (11) (1995) 1561–5.

[73] Trubetskaya A, Brown A, Tompsett GA, Timko MT, Umeki K, Kling J and etc., Characterization and reactivity of soot from fast pyrolysis of lignocellulosic compounds and monolignols, Applied Energy 212 (2018) 1489–500.

[74] Knudsen JN, Volatilization of Inorganic Matter during Combustion of Annual Biomass. PhD thesis, Technical University of Denmark, 2003.

[75] Dayton DC, Milne TA, Laboratory Measurements of Alkali Metal Containing Vapors Released during Biomass Combustion. In L. Baxter and R. DeSollar, Application of Advanced Technologies to Ash-Related Problems in Boilers, Plenum Press, 1996.

[76] Beeley T, Crelling J, Gibbins J, Hurt R, Lunden M, Man C and etc., Transient high-temperature thermal deactivation of momomaceral-rich coal chars, 26th Symp Comb Inst (1996) 3103–10.

[77] Franklin RE, Crystallite Growth in Graphitizing and Non-Graphitizing Carbons, Proc R Soc A Math Phys Eng Sci 209 (1951) 196–218.

[78] Oberlin A, Carbonization and graphitization, Carbon 22 (6) (1984) 521–41.

[79] Kurosaki F, Ishimaru K, Hata T, Bronsveld P, Kobayashi E, Imamura Y, Microstructure of wood charcoal prepared by flash heating, Carbon 41 (15) (2003) 3057–62.

[80] Jenkins GM, Kawamura K, Ban LL, Formation and structure of polymeric carbons, Proc R Soc Lond A 327 (1972) 501–17.

[81] Trubetskaya A, Jensen PA, Jensen JD, Steibel M, Spliethoff H, Glarborg P, Influence of fast pyrolysis conditions on yield and structural transformation of biomass chars, Fuel Process Tech 140 (2015) 205–14.

[82] Hata T, Ishimaru K, Fujisawa M, Bronsveld P, Vystavel T, De Hosson J and etc., Catalytic Graphitization of Wood-Based Carbons with Alumina by Pulse Current Heating, Full, Nano, Carbon Nano 13 (2005) 435–45.

[83] Johnson MT, Faber KT, Catalytic graphitization of three dimensional wood-derived porous scaffolds, J Mater Res 26 (1) (2011) 18–25.

[84] Gomez A, Silbermann R, Mahinpey N, A comprehensive experimental procedure for CO_2 coal gasification: Is there really a maximum reaction rate?, Appl Energy 137 (2015) 126–33.

[85] Gomez A, Mahinpey N, A new model to estimate CO_2 coal gasification kinetics based only on parent coal characterization properties, Appl Energy 137 (2015) 126–33.